Inverse Transfer Method Using Polymers with Various Functional Groups for Controllable Graphene Doping

Seong Kyu Lee,[†,⊥] Jae Won Yang,[‡,⊥] Hyun Ho Kim,[†] Sae Byeok Jo,[†] Boseok Kang,[†] Hyojin Bong,[†] Hyo Chan Lee,[†] Geunsik Lee,[‡] Kwang S. Kim,[§,*] and Kilwon Cho[†,*]

[†]Department of Chemical Engineering and [‡]Department of Chemistry, Pohang University of Science and Technology (POSTECH), Pohang, 790-784, Korea and [§]Department of Chemistry, Ulsan National Institute of Science and Technology (UNIST), Ulsan, 689-798, Korea. [⊥]S. K. Lee and J. W. Yang contributed equally to this work.

ABSTRACT The polymer-supported transfer of chemical vapor deposition (CVD)-grown graphene provides large-area and high-quality graphene on a target substrate; however, the polymer and organic solvent residues left by the transfer process hinder the application of CVD-grown graphene in electronic and photonic devices. Here, we describe an inverse transfer method (ITM) that permits the simultaneous transfer and doping of graphene without generating undesirable residues by using polymers with different functional groups. Unlike conventional wet transfer methods, the polymer supporting layer used in the ITM serves as a graphene doping layer placed at the interface between the graphene and the substrate. Polymers bearing functional groups can induce n-doping or p-doping into the graphene depending on the electron-donating or -withdrawing characteristics of functional groups. Theoretical models of dipole layer-induced graphene doping offered insights into the experimentally measured change in the work function and the Dirac point of the graphene. Finally, the electrical properties of pentacene field effect transistors prepared using graphene electrodes could be enhanced by employing the ITM to introduce a polymer layer that tuned the work function of graphene. The versatility of polymer functional groups suggests that the method developed here will provide valuable routes to the development of applications of CVD-grown graphene in organic electronic devices.

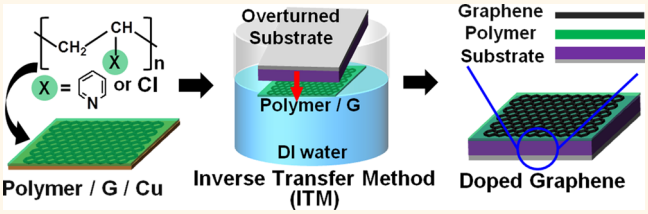

KEYWORDS: graphene · chemical vapor deposition · graphene transfer · contact doping · work function

Graphene displays remarkable properties that make it a promising material for use in next-generation soft electronics.[1−7] Chemical doping is essential for controlling the sheet resistance and work function of a graphene layer for use in high-performance graphene-based electronics and photonics.[8−12] Although atomic substitution,[13,14] molecular absorption,[15−18] and self-assembled monolayer[8,12,18,19] approaches have been applied to achieve graphene doping, none of these methods are simple and allow for the tunable doping of graphene. Polymer-supported transfer processes have been used to transfer as-synthesized graphene, grown using chemical vapor deposition (CVD), from a Cu foil to a target substrate.[20−23] Such transfer processes include applying a polymer coating, etching away the Cu layer, and removing the polymer layer. This process tends to introduce undesirable doping effects as a result of the polymer residue,[24−26] adsorbed organic solvent,[27] or both. A transfer process that does not cause an undesirable graphene doping effect is needed in the field.

Polymers are large molecules composed of repeating structural units and consist of a backbone and functional groups. Poly(methyl methacrylate) (PMMA) is widely used as a support layer in conventional graphene transfer process,[28,29] although most polymers may be used for this purpose.[25] The types and degree of graphene doping as a result of contact between a functionalized polymer and graphene can be tuned by employing polymers with

* Address correspondence to kwcho@postech.ac.kr; kimks@unist.ac.kr.

Received for review April 8, 2014 and accepted July 22, 2014.

Published online July 22, 2014
10.1021/nn503329s

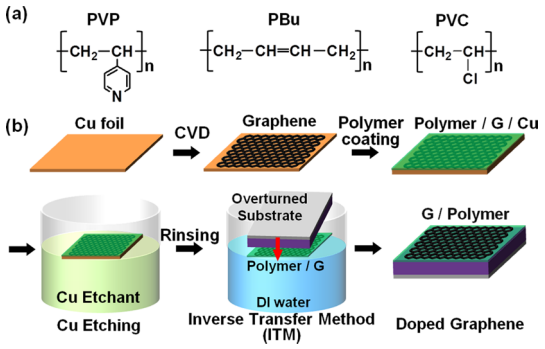

Figure 1. (a) Chemical structures of the poly(4-vinylpyridine) (PVP), polybutadiene (PBu), and poly(vinyl chloride) (PVC) polymers. (b) Schematic diagram of the process used for graphene growth and inverse transfer method using polymers.

various dipole moments. Graphene doping can, therefore, be controlled without introducing a contaminating residue by using a variety of polymers that simultaneously act as a support layer and a dopant during the transfer process.

We describe the development of a novel transfer method, the inverse transfer method (ITM), that uses different polymers with various functional groups to obtain residue-free doped graphene. The effects of the functional groups on graphene doping were investigated by testing poly(vinylpyridine) (PVP), polybutadiene (PBu), and poly(vinyl chloride) (PVC) as polymer supports, which yielded n-type doping, dedoping, or p-type doping of graphene (Figure 1a), respectively. These polymers have identical backbone structures and different functional groups at side chains. The doping effects resulting from the inversely transferred graphene were confirmed experimentally using Raman spectroscopy and ultraviolet photoelectron spectroscopy (UPS). Theoretical methods were used to model the polymer layers in contact with graphene and to calculate the change in the graphene dipole moment and work function as a result of contact with the polymer layer. The experimental and theoretical results supported a graphene doping mechanism involving metal-induced doping mediated by the surface dipole moment. ITM was then used to fabricate pentacene field effect transistors (FETs) with graphene electrodes that had been doped using polymers. The electrical performances of these FETs were compared.

RESULTS AND DISCUSSION

Graphene growth and the ITM entailed five steps (Figure 1b). In a typical wet transfer method involving PMMA, the PMMA/graphene film is placed onto a target substrate while the substrate is immersed in DI water. Because the graphene is covered with a PMMA layer, the transferred substrate must be dipped into an organic solvent to remove the PMMA layer. After this process, residual PMMA and organic solvent molecules on the graphene surface may cause unintentional graphene doping. The ITM, by contrast, involves the reverse transfer of the polymer/graphene film, as shown in Figure 1b. Unlike the conventional wet transfer process, the polymer supporting layer is placed at the interface between the graphene and the substrate. Because the polymer layer acts as a dopant and a supporting layer for the graphene, ITM does not require a polymer removal process. The transfer process is thereby simplified, and the transferred graphene is not contaminated by the presence of undesired polymer and the organic solvent residue (Figure S5). The doping type and magnitude could be stably controlled by using a polymer with the appropriate functional groups, as shown in Figure S1. The ITM process permits the tuning of the doping type and magnitude without the accumulation of contaminating residues.

The nature of graphene doping by the polymers used to transfer the graphene layer using the ITM was investigated using Raman spectroscopy and the UPS method. Raman spectroscopy is widely used to analyze the number of layers, quality, and doping of graphene.[30−33] The Raman spectrum of graphene generally displays three pronounced peaks: the D band, which is a first-order zone boundary phonon mode associated with defects in the graphene or graphene edge; the G band, which is a radial C−C stretching mode corresponding to the sp^2-bonded carbon atoms; and the 2D band, which is a second-order zone boundary phonon mode of graphene. The Raman spectrum of the graphene transferred using the ITM (Figure 2a) displays G- and 2D-bands but no D-band, indicating that high-quality monolayer graphene was successfully transferred to the SiO_2/Si substrate along with the polymer layer.

The graphene doping types obtained by conducting the ITM using three different polymers were identified through an analysis of the Raman spectra. Graphene doping introduced a blue-shift into the G-band and either a blue- or a red-shift into the 2D-band due to p-type or n-type doping, respectively.[30] The G-band positions obtained from PVP and PVC were blue-shifted with respect to PBu (Figure S7), indicating that the graphene was successfully doped. The 2D-band of the PVP was red-shifted relative to PBu, indicating that the PVP doping was n-type. The 2D-band of PVC was blue-shifted relative to PBu, indicating that the PVC doping was p-type. The ratio of the 2D-band intensity, I_{2D}, to the G-band intensity, I_G, and the full width at half-maximum (fwhm) of the G-band decreased as the dopant content in graphene increased.[30,31] The values of I_{2D}/I_G and the fwhm of the G-band were smaller from the PVP and PVC samples than from the PBu samples due to the presence of n-type or p-type doping, respectively (Figure 2b).

The work function was calculated from the UPS curve to characterize the type and magnitude of

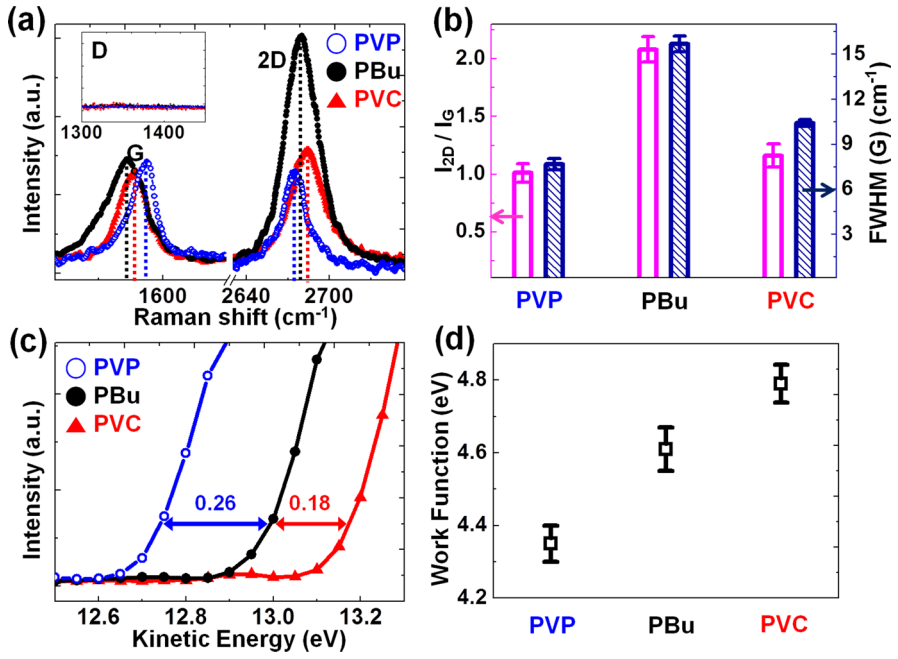

Figure 2. (a) Raman spectra of the monolayer graphene transferred onto a SiO_2/Si substrate using PVP, PBu, or PVC, *via* the inverse transfer method. The G-band (1588−1595 cm^{-1}) and 2D-band (2673−2684 cm^{-1}) shifted depending on the polymer identity. The inset shows the spectra around the D-band (1300−1450 cm^{-1}). (b) Graphene doping was confirmed by the reduced ratio of the 2D- and G-band intensities and by the reduced fwhm of the G-band. (c) UPS curves obtained from the graphene films prepared on different polymer layers, in the secondary electron emission region, or (d) the calculated work functions (4.35 eV for PVP, 4.61 eV for PBu, 4.79 eV for PVC).

doping. The graphene work function decreased for n-type[8] doping and increased for p-type[16] doping. The work function of the graphene on a polymer layer was calculated from the UPS data, as shown in Figure 2c and d. The work function was calculated using the following equation:

$$\Phi = \hbar\omega - |E_{sec} - E_{FE}| \quad (1)$$

where $\hbar\omega = 21.2$ eV (He I source), E_{sec} (eV) is the energy at which secondary emission begins, and E_{FE} (eV) is the Fermi edge (29.5 eV, obtained from the valence band spectrum, under a sample bias of −5 V). The use of different polymers in the ITM significantly altered the graphene work function (Figure 2d). The work function of graphene transferred using PBu, which did not affect the dipole moment due to the polymer's symmetric structure along the *z* axis, was calculated to be 4.61 eV. The work function of the graphene transferred using PVP, which includes pyridine functional groups, was found to be 4.35 eV. The work function decreased because graphene n-doping was induced by the dipole moment of the pyridine functional groups. The work function of the graphene transferred using PVC was found to be 4.79 eV. The work function increased because the dipole moment induced by the chlorine functional groups was oriented 180° relative to the dipole of the pyridine functional groups. The other properties of the graphene on the polymer layers (conductance, bending strength, and sheet resistance) were measured and are shown in Figure S6.

The mechanism underlying the effects of graphene doping by the polymers was investigated by performing theoretical calculations. The effects of the different polymer dipole moments on the graphene were examined using first-principles density functional theory (DFT) calculations.[34] The Wigner−Bardeen equation was used to analyze the work function, and we suggest a new mechanism for graphene doping by the polymer with the metal contact. Polymers with different functional groups were assumed to have a variety of dipole configurations. The change in polymer−graphene interface structures was caused by different dipole orientation induced by the different polymer on the graphene surfaces.

The work function of each optimized polymer−graphene interface structure was calculated and analyzed using the equation proposed by Wigner and Bardeen:

$$W = -\mu + D = -\mu - \frac{e}{\varepsilon_0} p \quad (2)$$

where μ is the chemical potential of the electrons caused by the mean electrostatic potential and *D* is related to the dipole barrier caused by a surface.[35] In the case of graphene, *D* in eq 2 vanishes due to the periodic symmetry of the graphene sp^2 hybridization orbital structure along the *z* axis. As a result, the work function of graphene is directly related to the chemical potential of graphene, which is consistent with the definition of the work function. By contrast, in the presence of polymers adsorbed onto the graphene

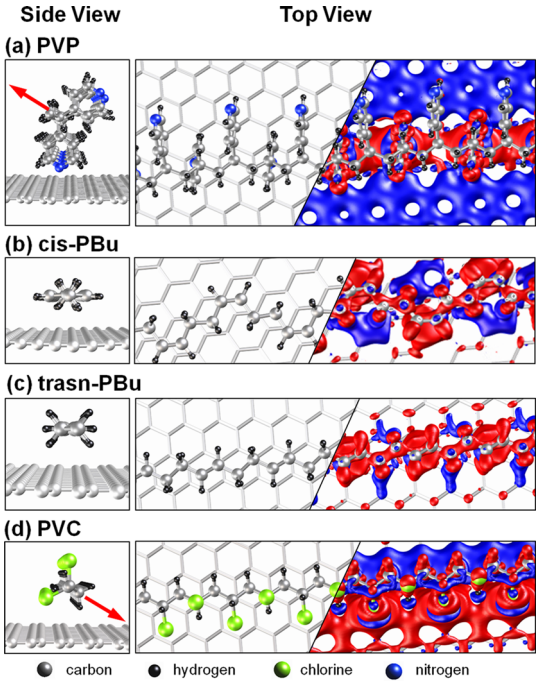

Figure 3. Side (left) and top (right) views of the optimized polymer–graphene interface structures and the electron density difference isosurface after the polymers had been adsorbed onto the graphene (gray: C atoms, black: H atoms, green: Cl atoms, blue: N atoms). A comparable crystallized polymer was used to model the polymer–graphene interface. (a) PVP on 6 × 6 graphene, (b) cis-PBu on 8 × 8 graphene, (c) trans-PBu on 4 × 4 graphene, and (d) PVC on 4 × 4 graphene. Red arrows: Directions of the dipole moments of the polymers. Cis-PBu and trans-PBu have no dipole moment because the electronic structures of these polymers are symmetric along the *z* direction. Top views of the electron density difference isosurface are plotted. Blue and red correspond to ±0.0006 e·Å^{-3}, indicating electron accumulation and depletion regions, respectively. The induced dipole moments at the interface depended on the direction of the polymer dipole moment.

surface, *D* does not disappear. The dipole moment perpendicular to the graphene surface may be calculated using the equation

$$p = -\frac{1}{A}\iint_{cell} dx\, dy \int dz\, \rho(x,y,z)z + \sum_i Z_i e z_i \quad (3)$$

where *A* is the area of a supercell normal to the *z* axis, ρ is the electron density, *i* indicates an ion, Z_i is the net atomic number of ion *i*, and z_i is the *z* coordinate of ion *i*. To better understand the effects of the surface-induced dipole moment on the work function of the interface, we calculated the change $\Delta\rho$ in the electron density caused by the adsorbed polymer according to the equation

$$\Delta\rho = \rho_{int} - (\rho_g + \rho_p) \quad (4)$$

where ρ_{int}, ρ_g, and ρ_p are the electron densities of the interface system, frozen graphene system, and frozen polymer system, respectively. Figure 3 shows the side (left) and top (right) view of the optimized polymer–graphene interface structures. The red arrows, in the side view, indicate the direction of the dipole moments of polymers. Because both the trans-PBu and cis-PBu have symmetric structures along the *z* direction, they do not have intrinsic dipole moments; however, PVC and PVP have intrinsic dipole moments due to the presence of their corresponding functional groups. The electron density difference isosurface of the polymer–graphene interface is plotted in the top view. $\Delta\rho$ depends on the direction of the dipole moment of each polymer. The dipole field p_p of the polymer determined the dipole moment p_{int} of the polymer–graphene interface, and the work function shift of graphene was caused by the dipole moment. The theoretically and experimentally determined work functions agreed qualitatively (Table 1). As the experimental binding structure of the polymer–graphene interface provided a different coverage and a broader spectrum of binding angles compared with our model interface structure, the calculated work function provides an upper limit of the work function of the doped graphene.

The theoretical results did not predict the experimentally observed change in the Dirac point with doping in Figure S1b. The calculated band structures for the polymer–graphene system indicated that the Fermi level lay at the Dirac point because the highest occupied molecular orbitals or the lowest unoccupied molecular orbitals of the polymers were far from the Fermi energy of graphene (Figure S8). Electrons could not easily hop between the graphene and polymer layers, as reported for graphene–SAM interfaces.[36] To check the doping effect of the polymer layer on the graphene in the polymer–graphene system, free-standing CVD-grown graphene was transferred by using a hole-patterned PMMA supporting layer (detailed process is shown in Figure S9). Figure 4a displays the optical microscope image of the transferred free-standing CVD-grown graphene onto the target substrate. The free-standing portion of the graphene (the inside of the PMMA hole) did not contact any polymer layers and/or metals during the entire transfer process. To demonstrate the polymer–graphene system, the free-standing graphene was transferred onto the PVP, PBu, or PVC spin-coated Si wafer. The doping effect of the polymer (spin-coated PVP, PBu, or PVC layer)–graphene (transferred free-standing graphene) system was evaluated by Raman spectra as shown in Figure 4b. Because the free-standing graphene was not doped, the Raman spectra depicted the G- and 2D-band of pristine graphene on the hexamethyldisiloxane (HMDS)-treated Si wafer (green). In the polymer–graphene system, the Raman spectrum of the transferred free-standing graphene onto the PVP (blue), PBu (black), or PVC (red) was not changed due to the absence of doping effect. The polymer–graphene system fabricated by direct spin-coating of the polymer layers on the transferred

TABLE 1. Calculation Results for the Polymer–Graphene Interface[a]

	graphene–polymer distance (Å)	adsorption energy (eV)	ρ_p (D)	ρ_{int} (D)	μ_{int} (eV)	W_{exp} (eV)	W_{int} (eV)
graphene					4.35		4.35
PVP	2.91 (G–N)	0.09	−0.64	−0.68	4.34	4.35	3.69
cis-PBu	2.54 (G–H)	0.10	0.01	0.10	4.36	4.61	4.41
trans-PBu	2.63 (G–H)	0.08	0.01	0.01	4.34		4.36
PVC	2.63 (G–H)	0.12	0.29	0.38	4.34	4.79	5.15

[a] The binding distance between graphene and polymer was calculated as the height difference between the graphene surface and the lowest atom belonging to the polymer (method in the SI). Symbols in parentheses of graphene–polymer distance denote the species of the closest atoms belonging to polymers. The dipole moment of each polymer was calculated from the isolated polymer.

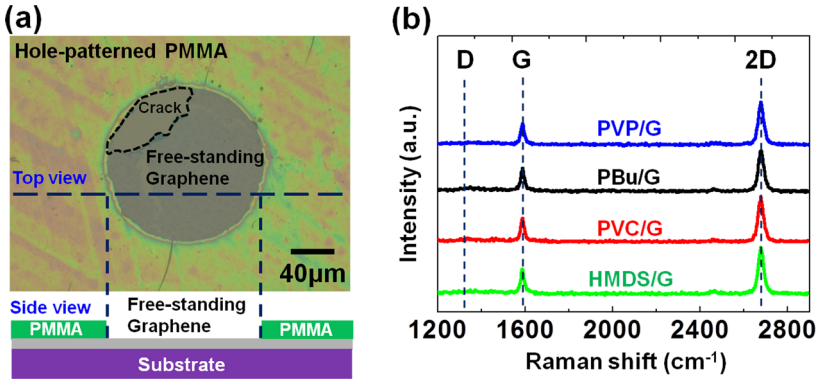

Figure 4. (a) Transferred free-standing graphene onto the target substrate by using hole-patterned PMMA. (b) Raman spectrum of the free-standing graphene transferred onto the PVP (blue), PBu (black), and PVC (red) spin-coated Si wafer and HMDS-treated Si wafer (green).

graphene also did not show a change of the Raman spectra (Figure S10). As a result, the doping behavior of graphene was not observed in the polymer–graphene system.

In the case of polymer–graphene–metal system, however, the Fermi level shift of graphene was observed. The model calculations in Figure S11 explained the graphene doping as resulting from a metal contact effect: a surface dipole moment of polymer-mediated graphene doping could be induced by metal contact, which provides an electron transport channel to the graphene as an electron reservoir. As shown in Figure 1b, in the ITM process, graphene was grown and contacted with the Cu foil, which included a high density of states near the Fermi energy of graphene. Then, the supporting/doping layer (PVP, PBu, or PVC) was spin-coated onto the graphene. In this step, electron transfer from the Cu foil to the graphene could be mediated by the polymer dipole moments. In contrast with general metals, single carbon monolayer graphene with a conical shape near the Dirac point creates a sensitive quantum capacitance.[37−40] Therefore, even a small number of transferred electrons under a dipole field can shift the graphene Fermi level upward or downward, and this shift will directly affect the work function of the graphene interface, as described in eq 2. Induced electron transfer tends to be preserved at the polymer–graphene interface after etching away the Cu foil due to the quantum capacitance properties of the graphene. In the case of Figure S1a, the Au electrodes on the graphene acted as an electron reservoir for the polymer–graphene–metal system, and the Dirac point of the graphene was changed.[27]

The graphene work function could be controlled by selecting an appropriate polymer; therefore, graphene electrodes doped by the polymers may be used to enhance the organic electronic device performance.[8,10,11] As one of the applications of ITM, bottom-contact pentacene FETs with graphene source/drain (S/D) electrodes doped by the polymers were fabricated to enhance the electrical performance (Figure S12). The morphologies of the pentacene films deposited onto the graphene electrodes prepared with different polymers and onto the hexamethyldisiloxane-treated SiO_2 dielectric layer were identical, as confirmed by scanning electron microscopy (Figure S13). The variations in the electrical properties of the devices, therefore, might result from the work function of the graphene electrode, which was controlled by the difference of the polymer layer.

Figure 5a–d show the electrical characteristics of pentacene FETs prepared with graphene electrodes transferred using PVP, PBu, or PVC, respectively. Figure 5a–c show the output characteristics of the pentacene FETs prepared with different graphene S/D electrodes doped by the polymers. The S-shaped non-ohmic behavior at a low drain voltage was remarkably reduced when the polymers in contact with graphene were switched from PVP (Figure 5a) to PVC (Figure 5c).

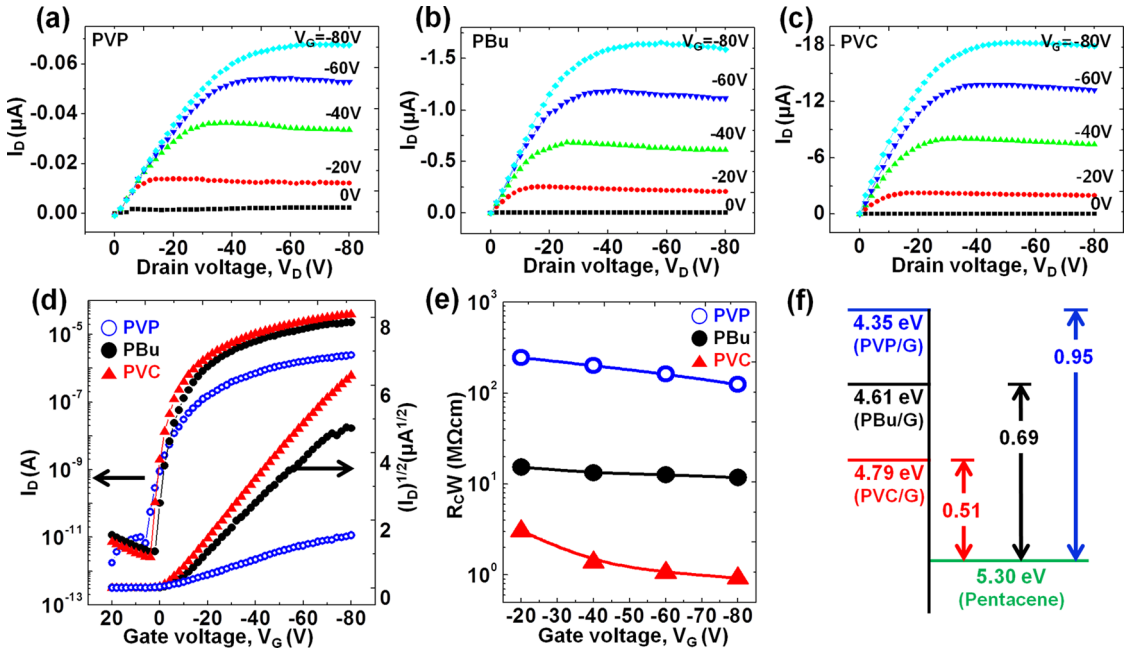

Figure 5. Output characteristics of pentacene FETs with graphene S/D on (a) PVP, (b) PBu, and (c) PVC. (d) Transfer characteristics of pentacene FETs with graphene S/D doped by the polymers. (e) Channel width-normalized contact resistances of the pentacene FETs. (f) Schematic energy levels of pentacene and doped graphene with different polymers; the change in hole injection barriers, which affects the pentacene FET field effect mobility, is shown as a control parameter of the work function of graphene with polymers.

Nonohmic behavior could be explained by the presence of a large injection barrier from the electrode to the channel due to a mismatch in the work function.[41]

Figure 5d shows a plot of the square root of $|I_D|$ in the saturation region of $V_D = -80$ V as a function of the gate voltage V_G, obtained from the fabricated device. The field effect mobility μ was calculated from the transfer characteristics measured for each of the 10−15 devices using the equation

$$|I_D| = \frac{W}{2L} C\mu(V_G - V_{Th})^2 \quad (5)$$

where $C = 1.08 \times 10^{-8}$ F·cm^{-2}, $W = 1000$ μm, and $L = 100$ μm. The calculated average field effect mobility was 0.2 ± 0.02 cm^2·(V·s)$^{-1}$ for PVC, 0.08 ± 0.04 cm^2·(V·s)$^{-1}$ for PBu, and 0.006 ± 0.002 cm^2·(V·s)$^{-1}$ for PVP. The pentacene FET performances obtained using the polymer/graphene electrodes were much better than those of identically structured FETs prepared with Au electrodes (0.015 cm^2·(V·s)$^{-1}$).[42] The devices were identical except for the polymers used during the ITM; therefore, the polymer-controlled hole injection barrier was responsible for the change in the field effect mobility.

The root of the field effect mobility effect was investigated by calculating the contact resistance R_C of each electrode using the transfer-line method with a channel length L that varied over the range 60−260 μm (at a constant channel width W of 1000 μm).[43,44] The contact resistance values were obtained from the intersection of the resistances at each gate voltage with $L = 0$, as calculated according to the equation

$$R_{total} = R_C + \frac{L}{WC_i\mu_i}(V_G - V_{T,i}) = R_C + R_{ch} \quad (6)$$

where μ_i is the intrinsic field effect mobility and $V_{T,i}$ is the threshold voltage. R_{total} was extracted from the inverse slope of each $I-V$ curve in the linear regime. The magnitudes of the channel width-normalized contact resistance R_CW of the graphene electrodes were ordered as follows: PVC < PBu < PVP (Figure 5e). Because the work function of graphene was increased to 4.79 eV though the use of the PVC layer, the graphene electrode with a high work function promoted hole injection (Figure 5f). The graphene electrodes prepared with PBu or PVP had lower work functions of 4.61 and 4.35 eV, which corresponded to high injection barriers and accordingly low field effect mobilities in the context of pentacene FETs.

CONCLUSIONS

In summary, a simple, easy, and controllable method for doping CVD-grown graphene was developed by using an ITM with polymers having different functional groups. A clean graphene film could be fabricated using the ITM without producing any unintentional doping from the polymer or organic solvent residue. The underlying polymer layer controllably doped the graphene layer. The doping characteristics obtained from polymers bearing different functional groups were examined experimentally and theoretically. The

performance of pentacene FETs could be enhanced by using an ITM with different polymers to tune the work function of the graphene electrodes. The versatility and flexibility of polymers available for use with the ITM process will enable the development of high-performance graphene-based organic electronics such as organic photovoltaics and organic light-emitting diodes.

METHODS/EXPERIMENTAL SECTION

Graphene Growth and Transfer. A Cu foil was placed in a quartz tube, and the foil surface was reduced by heating to 1000 °C under 10 standard cubic centimeters per minute (sccm) H_2 gas delivered at 50 mTorr over 1 h. Next, 45 sccm CH_4 gas was passed over the foil at 300 mTorr for 30 min. The quartz tube was then rapidly cooled. Polymer solutions containing 4.8 wt % PVP (M_w 160 kg mol^{-1}), 1.6 wt % PBu (M_w 180 kg mol^{-1}), or 1.4 wt % PVC (M_w 200 kg mol^{-1}) were spin-coated (~50 nm) onto one side of the graphene to form a supporting doping layer (Figure S3). The Cu foil was etched away using a 0.1 M ammonium persulfate ($(NH_4)_2S_2O_8$) solution. The remaining polymer/graphene film was then transferred to a deionized (DI) water bath for rinsing. The polymer/graphene film floated on the surfaces of the etchant and DI water after applying the copper foil etching process.

Characterization of the Cu Foil, the Polymer Layer, and the Graphene Surface. The morphologies of the Cu foil and the graphene films were characterized using atomic force microscopy (Digital Instruments Multimode) operating in tapping mode.

Properties of Graphene with Polymer Layers. Raman spectroscopy (Alpha300R, WITec, $\lambda = 532$ nm), ultraviolet photoelectron spectroscopy (4D, 8A2, and 10D beamline at the Pohang Accelerator Laboratory in Korea), UV−vis spectroscopy (Varian, CARY-5000), and characterization of the current−voltage properties of the FET devices, as measured using a Keithley 2636A semiconductor parameter analyzer, were performed.

Conflict of Interest: The authors declare no competing financial interest.

Acknowledgment. This work was supported by a grant (Code No. 2011-0031628) from the Center for Advanced Soft Electronics under the Global Frontier Research Program of the Ministry of Science, ICT & Future Planning, Korea, and NRF (National Honor Scientist Program: 2010-0020414). The authors thank the Pohang Accelerator Laboratory for providing the synchrotron radiation sources at the 4D, 8A2, and 10D beamlines used in this study.

Supporting Information Available: Additional information and figures. This material is available free of charge *via* Internet at http://pubs.acs.org.

REFERENCES AND NOTES

1. Novoselov, K. S.; Geim, A. K.; Morozov, S. V.; Jiang, D.; Katsnelson, M. I.; Grigorieva, I. V.; Dubonos, S. V.; Firsov, A. A. Two-Dimensional Gas of Massless Dirac Fermions in Graphene. *Nature* **2005**, *438*, 197–200.
2. Lee, C.; Wei, X. D.; Kysar, J. W.; Hone, J. Measurement of the Elastic Properties and Intrinsic Strength of Monolayer Graphene. *Science* **2008**, *321*, 385–388.
3. Zhang, Y. B.; Tan, Y. W.; Stormer, H. L.; Kim, P. Experimental Observation of the Quantum Hall Effect and Berry's Phase in Graphene. *Nature* **2005**, *438*, 201–204.
4. Georgakilas, V.; Otyepka, M.; Bourlinos, A. B.; Chandra, V.; Kim, N.; Kemp, K. C.; Hobza, P.; Zboril, R.; Kim, K. S. Functionalization of Graphene: Covalent and Non-Covalent Approaches, Derivatives and Applications. *Chem. Rev.* **2012**, *112*, 6156–6214.
5. Eda, G.; Fanchini, G.; Chhowalla, M. Large-Area Ultrathin Films of Reduced Graphene Oxide as a Transparent and Flexible Electronic Material. *Nat. Nanotechnol.* **2008**, *3*, 270–274.
6. Hossain, M. Z.; Johns, J. E.; Bevan, K. H.; Karmel, H. J.; Liang, Y. T.; Yoshimoto, S.; Mukai, K.; Koitaya, T.; Yoshinobu, J.; Kawai, M.; *et al*. Chemically Homogeneous and Thermally Reversible Oxidation of Epitaxial Graphene. *Nat. Chem.* **2012**, *4*, 305–309.
7. Li, N.; Chen, Z. P.; Ren, W. C.; Li, F.; Cheng, H. M. Flexible Graphene-Based Lithium Ion Batteries with Ultrafast Charge and Discharge Rates. *Proc. Natl. Acad. Sci. U.S.A.* **2012**, *109*, 17360–17365.
8. Park, J.; Lee, W. H.; Huh, S.; Sim, S. H.; Kim, S. B.; Cho, K.; Hong, B. H.; Kim, K. S. Work-Function Engineering of Graphene Electrodes by Self-Assembled Monolayers for High-Performance Organic Field-Effect Transistors. *J. Phys. Chem. Lett.* **2011**, *2*, 841–845.
9. Hsu, C. L.; Lin, C. T.; Huang, J. H.; Chu, C. W.; Wei, K. H.; Li, L. J. Layer-By-Layer Graphene/TCNQ Stacked Films as Conducting Anodes for Organic Solar Cells. *ACS Nano* **2012**, *6*, 5031–5039.
10. Han, T. H.; Lee, Y.; Choi, M. R.; Woo, S. H.; Bae, S. H.; Hong, B. H.; Ahn, J. H.; Lee, T. W. Extremely Efficient Flexible Organic Light-Emitting Diodes with Modified Graphene Anode. *Nat. Photonics* **2012**, *6*, 105–110.
11. Jo, G.; Na, S. I.; Oh, S. H.; Lee, S.; Kim, T. S.; Wang, G.; Choe, M.; Park, W.; Yoon, J.; Kim, D. Y.; *et al*. Tuning of a Graphene-Electrode Work Function to Enhance the Efficiency of Organic Bulk Heterojunction Photovoltaic Cells with an Inverted Structure. *Appl. Phys. Lett.* **2010**, *97*, 213301.
12. Kang, B.; Lim, S.; Lee, W. H.; Jo, S. B.; Cho, K. Work-Function-Tuned Reduced Graphene Oxide *via* Direct Surface Functionalization as Source/Drain Electrodes in Bottom-Contact Organic Transistors. *Adv. Mater.* **2013**, *41*, 5856–5862.
13. Wei, D. C.; Liu, Y. Q.; Wang, Y.; Zhang, H. L.; Huang, L. P.; Yu, G. Synthesis of N-Doped Graphene by Chemical Vapor Deposition and Its Electrical Properties. *Nano Lett.* **2009**, *9*, 1752–1758.
14. Jin, Z.; Yao, J.; Kittrell, C.; Tour, J. M. Large-Scale Growth and Characterizations of Nitrogen-Doped Monolayer Graphene Sheets. *ACS Nano* **2011**, *5*, 4112–4117.
15. Dong, X. C.; Fu, D. L.; Fang, W. J.; Shi, Y. M.; Chen, P.; Li, L. J. Doping Single-Layer Graphene with Aromatic Molecules. *Small* **2009**, *5*, 1422–1426.
16. Chen, W.; Chen, S.; Qi, D. C.; Gao, X. Y.; Wee, A. T. S. Surface Transfer p-Type Doping of Epitaxial Graphene. *J. Am. Chem. Soc.* **2007**, *129*, 10418–10422.
17. Gunes, F.; Shin, H. J.; Biswas, C.; Han, G. H.; Kim, E. S.; Chae, S. J.; Choi, J. Y.; Lee, Y. H. Layer-By-Layer Doping of Few-Layer Graphene Film. *ACS Nano* **2010**, *4*, 4595–4600.
18. Park, J.; Jo, S. B.; Yu, Y. J.; Kim, Y.; Yang, W.; Lee, W. H.; Kim, H. H.; Hong, B. H.; Kim, P.; Cho, K.; *et al*. Single-Gate Bandgap Opening of Bilayer Graphene by Dual Molecular Doping. *Adv. Mater.* **2012**, *24*, 407–411.
19. Lee, B.; Chen, Y.; Duerr, F.; Mastrogiovanni, D.; Garfunkel, E.; Andrei, E. Y.; Podzorov, V. Modification of Electronic Properties of Graphene with Self-Assembled Monolayers. *Nano Lett.* **2010**, *10*, 2427–2432.
20. Kim, K. S.; Zhao, Y.; Jang, H.; Lee, S. Y.; Kim, J. M.; Kim, K. S.; Ahn, J. H.; Kim, P.; Choi, J. Y.; Hong, B. H. Large-Scale Pattern Growth of Graphene Films for Stretchable Transparent Electrodes. *Nature* **2009**, *457*, 706–710.
21. Li, X. S.; Cai, W. W.; An, J. H.; Kim, S.; Nah, J.; Yang, D. X.; Piner, R.; Velamakanni, A.; Jung, I.; Tutuc, E.; *et al*. Large-Area Synthesis of High-Quality and Uniform Graphene Films on Copper Foils. *Science* **2009**, *324*, 1312–1314.
22. Bae, S.; Kim, H.; Lee, Y.; Xu, X. F.; Park, J. S.; Zheng, Y.; Balakrishnan, J.; Lei, T.; Kim, H. R.; Song, Y. I.; *et al*. Roll-To-Roll Production of 30-Inch Graphene Films for Transparent Electrodes. *Nat. Nanotechnol.* **2010**, *5*, 574–578.

23. Gao, L.; Ni, G. X.; Liu, Y.; Liu, B.; Castro Neto, A. H.; Loh, K. P. Face-To-Face Transfer of Wafer-Scale Graphene Films. *Nature* **2014**, *505*, 190–194.
24. Pirkle, A.; Chan, J.; Venugopal, A.; Hinojos, D.; Magnuson, C. W.; McDonnell, S.; Colombo, L.; Vogel, E. M.; Ruoff, R. S.; Wallace, R. M. The Effect of Chemical Residues on the Physical and Electrical Properties of Chemical Vapor Deposited Graphene Transferred to SiO_2. *Appl. Phys. Lett.* **2011**, *99*, 122108.
25. Lee, W. H.; Suk, J. W.; Lee, J.; Hao, Y.; Park, J.; Yang, J. W.; Ha, H.-W.; Murali, S.; Chou, H.; Akinwande, D.; *et al*. Simultaneous Transfer and Doping of CVD-Grown Graphene by Fluoropolymer for Transparent Conductive Films on Plastic. *ACS Nano* **2012**, *6*, 1284–1290.
26. Lee, W. H.; Park, J.; Sim, S. H.; Lim, S.; Kim, K. S.; Hong, B. H.; Cho, K. Surface-Directed Molecular Assembly of Pentacene on Monolayer Graphene for High-Performance Organic Transistors. *J. Am. Chem. Soc.* **2011**, *133*, 4447–4454.
27. Kim, H. H.; Yang, J. W.; Jo, S. B.; Kang, B.; Lee, S. K.; Bong, H.; Lee, G.; Kim, K. S.; Cho, K. Substrate-Induced Solvent Intercalation for Stable Graphene Doping. *ACS Nano* **2013**, *7*, 1155–1162.
28. Lee, W. H.; Park, J.; Sim, S. H.; Jo, S. B.; Kim, K. S.; Hong, B. H.; Cho, K. Transparent Flexible Organic Transistors Based on Monolayer Graphene Electrodes on Plastic. *Adv. Mater.* **2011**, *23*, 1752–1756.
29. Lee, W. H.; Park, J.; Kim, Y.; Kim, K. S.; Hong, B. H.; Cho, K. Control of Graphene Field-Effect Transistors by Interfacial Hydrophobic Self-Assembled Monolayers. *Adv. Mater.* **2011**, *23*, 3460–3464.
30. Das, A.; Pisana, S.; Chakraborty, B.; Piscanec, S.; Saha, S. K.; Waghmare, U. V.; Novoselov, K. S.; Krishnamurthy, H. R.; Geim, A. K.; Ferrari, A. C.; *et al*. Monitoring Dopants by Raman Scattering in an Electrochemically Top-Gated Graphene Transistor. *Nat. Nanotechnol.* **2008**, *3*, 210–215.
31. Casiraghi, C. Doping Dependence of the Raman Peaks Intensity of Graphene Close to the Dirac Point. *Phys. Rev. B* **2009**, *80*, 233407.
32. Ferrari, A. C.; Meyer, J. C.; Scardaci, V.; Casiraghi, C.; Lazzeri, M.; Mauri, F.; Piscanec, S.; Jiang, D.; Novoselov, K. S.; Roth, S.; *et al*. Raman Spectrum of Graphene and Graphene Layers. *Phys. Rev. Lett.* **2006**, *97*, 187401.
33. Wang, Y. Y.; Ni, Z. H.; Yu, T.; Shen, Z. X.; Wang, H. M.; Wu, Y. H.; Chen, W.; Wee, A. T. S. Raman Studies of Monolayer Graphene: The Substrate Effect. *J. Phys. Chem. C* **2008**, *112*, 10637–10640.
34. Yang, J. W.; Lee, G.; Kim, J. S.; Kim, K. S. Gap Opening of Graphene by Dual $FeCl_3$-Acceptor and K-Donor Doping. *J. Phys. Chem. Lett.* **2011**, *2*, 2577–2581.
35. Leung, T. C.; Kao, C. L.; Su, W. S.; Feng, Y. J.; Chan, C. T. Relationship between Surface Dipole, Work Function and Charge Transfer: Some Exceptions to an Established Rule. *Phys. Rev. B* **2003**, *68*, 195408.
36. Yokota, K.; Takai, K.; Enoki, T. Carrier Control of Graphene Driven by the Proximity Effect of Functionalized Self-Assembled Monolayers. *Nano Lett.* **2011**, *11*, 3669–3675.
37. Xia, J. L.; Chen, F.; Li, J. H.; Tao, N. J. Measurement of the Quantum Capacitance of Graphene. *Nat. Nanotechnol.* **2009**, *4*, 505–509.
38. Droscher, S.; Roulleau, P.; Molitor, F.; Studerus, P.; Stampfer, C.; Ensslin, K.; Ihn, T. Quantum Capacitance and Density of States of Graphene. *Appl. Phys. Lett.* **2010**, *96*, 014009.
39. Yu, G. L.; Jalil, R.; Belle, B.; Mayorov, A. S.; Blake, P.; Schedin, F.; Morozov, S. V.; Ponomarenko, L. A.; Chiappini, F.; Wiedmann, S.; *et al*. Interaction Phenomena in Graphene Seen through Quantum Capacitance. *Proc. Natl. Acad. Sci. U.S.A.* **2013**, *110*, 3282–3286.
40. Fang, T.; Konar, A.; Xing, H. L.; Jena, D. Carrier Statistics and Quantum Capacitance of Graphene Sheets and Ribbons. *Appl. Phys. Lett.* **2007**, *91*, 092109.
41. Ishii, H.; Sugiyama, K.; Ito, E.; Seki, K. Energy Level Alignment and Interfacial Electronic Structures at Organic-Metal and Organic-Organic Interfaces. *Adv. Mater.* **1999**, *11*, 605–625.
42. Lim, S.; Kang, B.; Kwak, D.; Lee, W. H.; Lim, J. A.; Cho, K. Inkjet-Printed Reduced Graphene Oxide/Poly(Vinyl Alcohol) Composite Electrodes for Flexible Transparent Organic Field-Effect Transistors. *J. Phys. Chem. C* **2012**, *116*, 7520–7525.
43. Cho, J. H.; Kim, D. H.; Jang, Y.; Lee, W. H.; Ihm, K.; Han, J. H.; Chung, S.; Cho, K. Effects of Metal Penetration into Organic Semiconductors on the Electrical Properties of Organic Thin Film Transistors. *Appl. Phys. Lett.* **2006**, *89*, 132101.
44. Lim, J. A.; Cho, J. H.; Park, Y. D.; Kim, D. H.; Hwang, M.; Cho, K. Solvent Effect of Inkjet Printed Source/Drain Electrodes on Electrical Properties of Polymer Thin-Film Transistors. *Appl. Phys. Lett.* **2006**, *88*, 082102.